Energy-transfer processes in $Y_3Al_5O_{12}$:Tm,Ho

Valentina A. French, Roger R. Petrin, and Richard C. Powell
Center for Laser Research, Oklahoma State University, Stillwater, Oklahoma 74078

Milan Kokta
Union Carbide, Washougal, Washington 98671
(Received 16 April 1992)

The characteristics of energy transfer and migration processes important in the optical dynamics of $Y_3Al_5O_{12}$:Tm,Ho and $Y_3Al_5O_{12}$:Tm laser crystals were investigated. Laser-induced grating spectroscopy was used to study spatial migration of energy among the Tm ions as a function of both temperature and Tm ion concentration. The presence of energy migration was identified in the $^3H_4$ level, and this was shown to enhance the cross-relaxation process from this level. Efficient long-range energy migration was found to take place in the $^3F_4$ level, which enhances the energy transfer to Ho^{3+} ions. The parameters describing excitation migration were determined experimentally and used to calculate an overall Tm-Ho energy transfer rate. This was found to be in close agreement with the rate determined by the results of fluorescence spectral dynamics measurements. Theoretical estimates were made of the fundamental ion-ion interaction rates responsible for each of the physicsl processes investigated here and the results were all found to be in close agreement with the experimentally determined values.

I. INTRODUCTION

The development of room-temperature lasers based on $Y_3Al_5O_{12}:Tm^{3+},Ho^{3+}$ (Tm,Ho:YAG) crystals has led to a renewed interest in the optical properties of this material. As a result, a significant amount of work has been done in recent years on measuring the spectroscopic and lasing properties of the Tm,Ho:YAG system.[1-6] The previous research has identified a complex chain of physical processes by which the pump photon energy is transferred from the Tm^{3+} to the Ho^{3+} ions. These processes are shown in Fig. 1. In a diode laser-pumped Tm,Ho:YAG laser, the $^3H_4$ level of the Tm ions is directly excited by the pump energy. This is followed by a cross-relaxation process between neighboring Tm ions which gives rise to two Tm ions in the $^3F_4$ level for each photon absorbed in the $^3H_4$ level. There is spatial energy migration among the Tm ions in the $^3F_4$ level followed by direct transfer of energy from this level to the Ho $^5I_7$ level.[1] It has also been suggested that an additional spatial energy migration process may occur in the $^3H_4$ level of the Tm ions in samples of high Tm concentration.[2] The properties of these complex processes have not been well characterized. Previous studies focused on the initial Tm cross-relaxation process[3,4] or on the overall Tm-Ho energy transfer efficiency.[7,8] A detailed understanding of the energy transfer processes in Tm,Ho:YAG crystals is important for modeling the optical pumping dynamics of these lasers in order to understand their operational properties and to optimize dopant concentrations to increase the efficiency of laser operation.

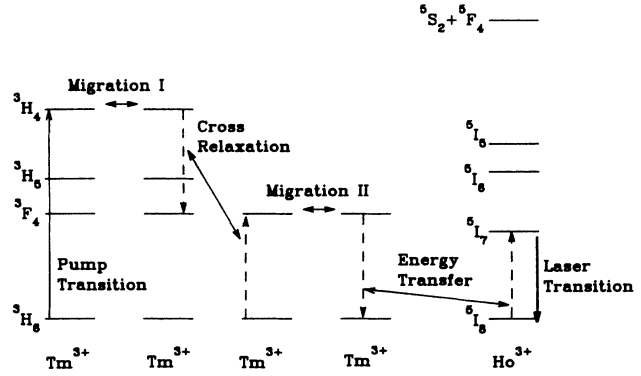

FIG. 1. Energy transfer processes in Tm,Ho:YAG.

In the work described here we present the results of a comprehensive study of energy transfer processes in Tm,Ho:YAG. Special consideration is given to the energy migration processes, which have received little attention in previous research. The fundamental properties of these processes can be accurately explained through theoretical models of ion-ion interaction mechanisms. The overall Tm-Ho energy transfer rate predicted as a result of sequential relaxation, migration, and trapping processes is shown to be consistent with the experimentally measured values.

II. EXPERIMENTAL

The samples used in this work are Tm,Ho:YAG, Tm:YAG, and Ho:YAG crystals with different dopant concentrations, grown by the standard Czochralski technique. The dopant concentration of each sample is listed in Table I.

The experiments performed include the measurement of optical absorption and emission spectra, transient fluorescence decay measurements, and laser-induced grating measurements. For the emission spectra measurements, either an argon-ion laser tuned to the 465.8-nm line, or an alexandrite laser tuned to 765 nm, were used

TABLE I. Concentrations of samples used in this study.

Sample no.	Concentrations (cm^{-3}) Tm^{3+}	Ho^{3+}
1	14.1×10^{20}	
2	8.2×10^{20}	0.69×10^{20}
3	5.6×10^{20}	
4	0.14×10^{20}	
5		0.69×10^{20}

to resonantly excite Tm ions in the $^1G_4$ or $^3H_4$ level, respectively. The near-infrared emission spectra were obtained using a 0.22-m Spex model 1681B spectrometer with gratings blazed at 1.25 μm and 2 μm, and a PbS detector. In the visible spectral region, emission spectra were obtained using a Spex 0.85-m double spectrometer with a 500-nm blazed grating and a Hammamatsu R446 photomultiplier tube. All emission spectra were corrected for grating and detector response.

For the transient emission decay measurements a nitrogen laser-pumped dye laser with an approximately 10-ns pulse duration was used to excite the $^1G_4$ level of the Tm ions. For all transient emission measurements the signal from the detector was averaged by an EG&G boxcar averager and stored on a computer.

The absorption spectra were obtained using a computer-controlled Carry 2400 spectrophotometer. For the low-temperature measurements the samples were mounted in a cryostat and the temperature was controlled using a closed cycle helium refrigerator and a Lake Shore temperature controller.

The laser-induced grating (LIG) spectroscopy measurements were performed using nondegenerate four-wave-mixing techniques to write and probe transient population gratings of Tm ions in the $^3F_4$ energy level. The output of an argon-ion laser tuned to the 465.8-nm line was split into two beams (write beams) of equal intensity and path lengths. These beams were focused and crossed inside the sample at an angle θ to form a sine wave interference pattern. Through optical absorption this interference pattern created a spatial population distribution of the Tm ions in the $^3F_4$ metastable state with the same pattern. This population distribution acted as a refractive-index grating due to the polarizability difference of the ions in the excited state versus the ground state.[9] To probe the properties of this LIG the output of a He-Ne laser was focused on the grating and carefully aligned to satisfy the Bragg scattering condition. The signal beam was detected by an RCA C31034 photomultiplier tube, averaged by an EG&G signal averager and stored on a computer. For the LIG transient decay measurements, the write beams were mechanically chopped off and on.

III. RESULTS

Room-temperature absorption and emission spectra for transitions between the $^3H_4$-$^3H_6$ levels of the Tm ions were measured using sample 1. Figure 2 shows the normalized emission and absorption spectra of these transitions. These are the spectra needed to determine an ion-ion interaction rate for Tm energy migration in the $^3H_4$ level. The emission spectra were recorded after excitation at 765 nm using the alexandrite laser. Figure 3 shows the concentration dependence of the fluorescence quantum efficiency of the $^3H_4$ multiplet. The data

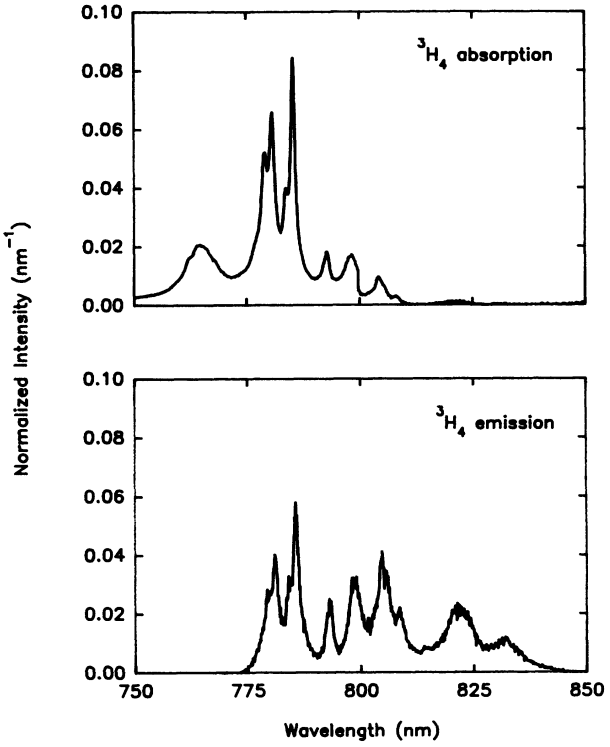

FIG. 2. Normalized emission and absorption spectra of the transitions involving the Tm $^3H_4$ level at room temperature.

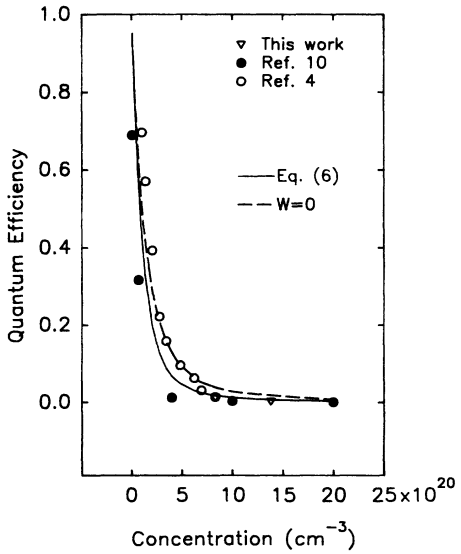

FIG. 3. Variation of the fluorescence quantum efficiency of the Tm $^3H_4$ level with the Tm ion concentration at room temperature. Triangles—experimental values determined in this work; squares—data from Ref. 8; circles—data from Ref. 4. Solid and broken lines are theoretical predictions.

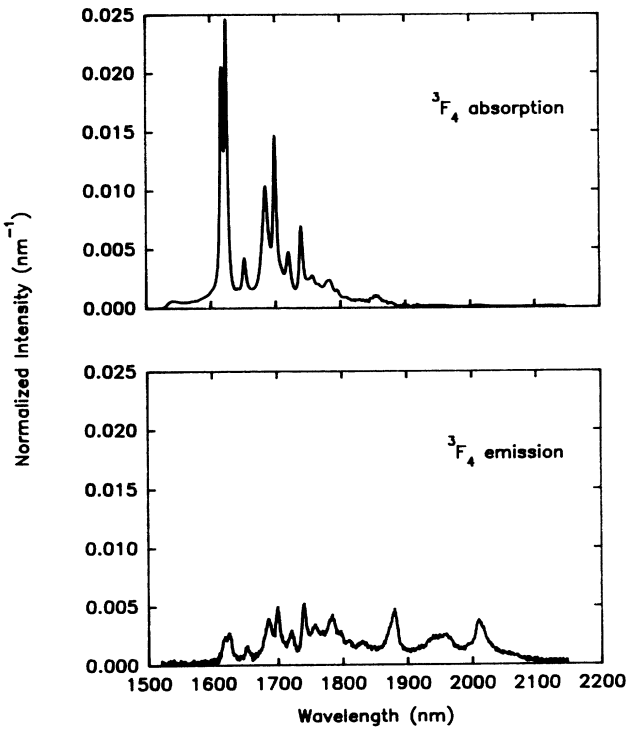

FIG. 4. Normalized emission and absorption spectra of the transitions involving the Tm $^3F_4$ level at room temperature.

represent a combination of the results obtained here and those of several other researchers.[4,10] The solid and broken lines represent the theoretical predictions described in the following section.

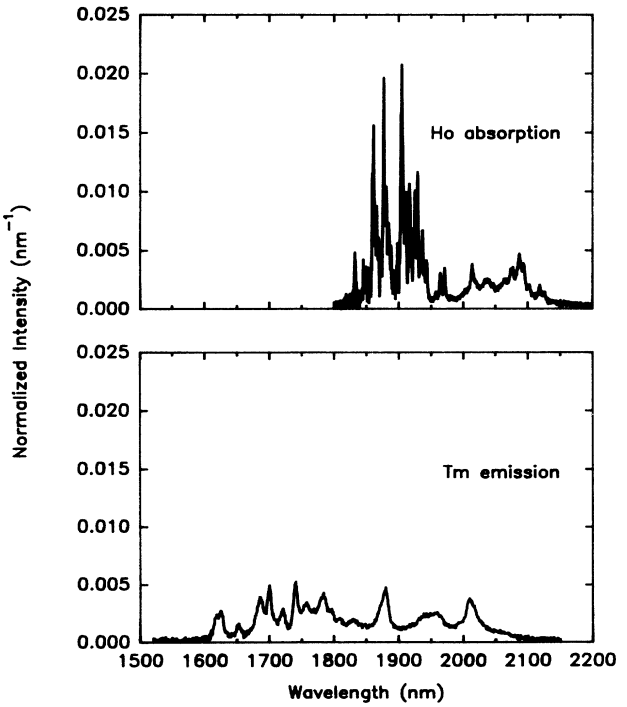

FIG. 5. Normalized emission and absorption spectra of the transitions involving the Tm $^3F_4$ and Ho $^5I_7$ energy levels, respectively, at room temperature.

Room-temperature emission and absorption spectra due to transitions associated with the $^3F_4$ energy level of Tm^{3+}, and absorption spectra due to transitions associated with the $^5I_7$ energy level of Ho^{3+}, were measured using samples 1 and 5, respectively. Figures 4 and 5 show the normalized emission and absorption spectra for these transitions. These are the spectra needed to determine the ion-ion interaction rates for energy migration among the Tm^{3+} ions in the $^3F_4$ level and for the Tm-Ho energy transfer.

Low-temperature emission and absorption spectra associated with transitions involving the $^3F_4$ level of Tm were obtained using sample 1. Figure 6 shows the normalized emission and absorption spectra of these transitions at a temperature of 12 K. These spectra are needed to understand the temperature dependence of the energy migration among Tm^{3+} ions in the $^3F_4$ level.

Laser-induced grating decay kinetics were measured in samples 1, 2, and 3 for different grating spacings and different temperatures. No LIG signal was detected in sample 4 for write beams crossing angles greater than 3°, probably due to the very low concentration of Tm ions in this sample. The decay kinetics were found to be exponential, and consistent with the fluorescence decay dynamics of the Tm $^3F_4$ metastable level in each of the samples investigated. This shows that for these excitation conditions the LIG signals are associated with transient population gratings of Tm^{3+} ions in this metastable level. The LIG signal transient decays were found to be dependent on the grating spacing in all three samples, indicating the presence of long-range energy migration. This dependence weakens considerably at low temperatures, implying lower migration rates at these temperatures.

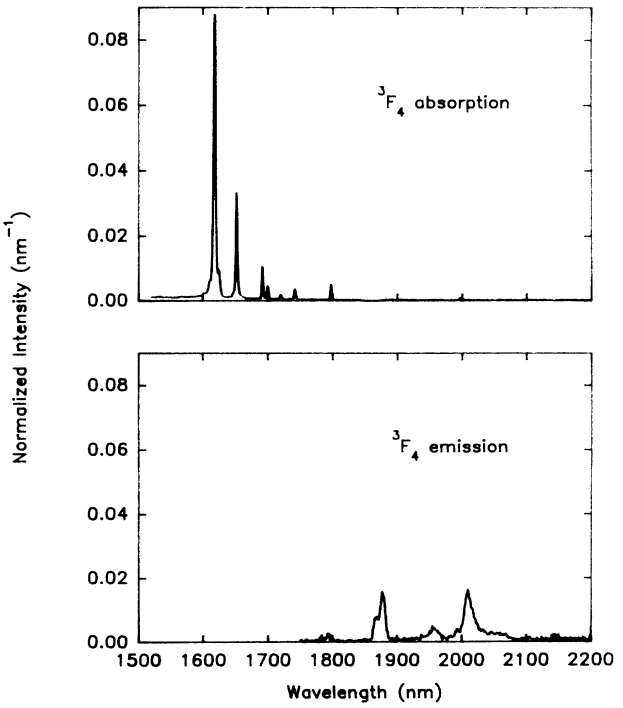

FIG. 6. Normalized emission and absorption spectra of the transitions involving the Tm $^3F_4$ level at a temperature of 12 K.

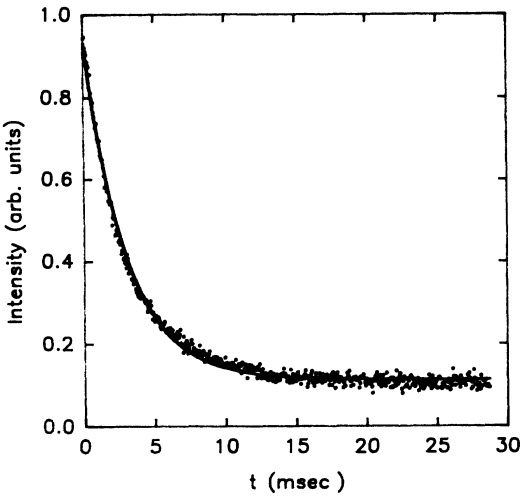

FIG. 7. LIG transient decay pattern from sample 1 at room temperature and a grating spacing of 3.3 μm. Solid circles—experimental points, solid line—theoretical fit.

Figure 7 shows a typical LIG transient decay curve at room temperature and a grating spacing of 3.3 μm (i.e., a crossing angle between the write beams of 8°). The solid circles represent experimental points, and the solid line is the theoretical prediction discussed in the following section.

IV. INTERPRETATION

The measured absorption and emission spectra described in the previous section can be used to calculate spectral overlap integrals needed to predict the critical interaction distances associated with the ion-ion interaction rates. The critical interaction distance represents the distance around the excited donor ion at which the nonradiative energy transfer rate is equal to the intrinsic decay rate of the donor.

For a nonradiative electric dipole-dipole ion-ion interaction mechanism, the critical interaction distance is given by[11]

$$R_{DX}^6=(3/4\pi)(\hbar c/n)^4 Q_X \int \lambda^6 f_D^{\rm em}(\lambda) f_X^{\rm abs}(\lambda) d\lambda \ , \quad (1)$$

where $X=D$ (for donor-donor transfer) or A (for donor-acceptor transfer), n is the refractive index of the material, $f_D^{\rm em}(\lambda)$ and $f_X^{\rm abs}(\lambda)$ are the normalized emission and absorption spectra, respectively [i.e., $\int f_D^{\rm em}(\lambda)d\lambda=1$; $\int f_X^{\rm abs}(\lambda)d\lambda=1$], and Q_X is the integrated absorption cross section [i.e., $Q_X=\int \sigma_X(E)dE$ where σ_X is the absorption cross section of ion X]. Using Eq. (1) and the spectra presented in the previous section, the critical interaction distances for the Tm-Tm and Tm-Ho interaction processes were calculated. These values are listed in Table II.

TABLE II. Critical interaction distances calculated in this work.

Energy transfer process	$R_{\rm crit.}$ (Å)	Temperature (K)
Tm $^3H_4$-Tm $^3H_4$	10.3	293
Tm $^3F_4$-Tm $^3F_4$	16.0	293
Tm $^3F_4$-Tm $^3F_4$	11.5	12
Tm $^3F_4$-Ho $^5I_7$	17.3	293

A. Tm-Tm energy migration in the $^3H_4$ level

The concentration dependence of the fluorescence lifetime of the $^3H_4$ multiplet of Tm^{3+} has been studied previously,[4,10] and the observed concentration quenching is generally attributed to a cross-relaxation process with a neighboring Tm^{3+} ion leaving both ions in their $^3F_4$ metastable states. However, a possible competing process for concentration quenching is energy migration occurring within the $^3H_4$ level of Tm^{3+} and eventual energy loss at a quenching site. The competition between these two types of quenching processes is considered here.

The fluorescence quantum efficiency of emission from the $^3H_4$ level can be determined from

$$\eta=A_r/A_m \ , \quad (2)$$

where A_r is the predicted radiative relaxation rate and A_m is the measured fluorescence decay rate. The predicted radiative lifetime[12] is 790 μs giving a predicted radiative transition rate of 1270 s^{-1}. The concentration dependence of the fluorescence quantum efficiency is shown in Fig. 3. The solid line is the theoretical prediction for the fluorescence quantum efficiency determined by the method discussed below.

The two possible types of ion-ion interactions leading to the quenching of the fluorescence from the $^3H_4$ level are the cross-relaxation and the migration enhanced cross-relaxation mechanisms. The time evolution of the intensity of the fluorescence emission from the $^3H_4$ level can be written as[13]

$$I(t)=I(0)\exp[-(A_r t+\gamma t^{1/2}+Wt)] \ , \quad (3)$$

where $I(0)$ is the initial intensity, γ is a parameter describing the ion-ion cross-relaxation interaction without migration, and W is the migration enhanced cross-relaxation rate. The parameter γ has the form described by Forster for fluorescence decay of a randomly distributed ensemble of ions interacting through an electric dipole-dipole mechanism,[14]

$$\gamma=\tfrac{4}{3}(\pi)^{3/2} n_{\rm Tm} R_{\rm cr}^3 A_r^{1/2} \ . \quad (4)$$

Here $R_{\rm cr}$ is the critical interaction distance between two Tm^{3+} ions for the cross-relaxation mechanism, and $n_{\rm Tm}$ is the concentration of Tm ions. The migration enhanced cross-relaxation rate has the form determined by Burshtein[15]

$$W=\pi(2\pi/3)^{5/2} R_{\rm cr}^3 R_{\rm mig}^3 n_{\rm Tm}^2 A_r \ , \quad (5)$$

where $R_{\rm mig}$ is the critical interaction distance between Tm^{3+} ions for energy migration. Again it is assumed that electric dipole-dipole interaction is responsible for both the migration steps and the final quenching step.

Equations (4) and (5) reflect the fact that, for the case of interest here, both the donors and acceptors are Tm ions.

Following the development in Ref. 13, Eq. (3) can be used to obtain an expression for the fluorescence quantum efficiency,

$$\eta=[A_r/(A_r+W)]\{1-\pi^{1/2}x\exp(x^2)[1-\mathrm{erf}(x)]\}\ , \tag{6}$$

where

$$x=\gamma/[2(A_r+W)^{1/2}]\ . \tag{7}$$

The only unknown quantities in Eqs. (3)–(7) are the critical interaction distances. Once these are determined the fluorescence quantum efficiency can be predicted from Eq. (6). These critical interaction distances can be found from spectral overlap data. Using the spectra in Fig. 2 and Eq. (1), R_{mig} was found to be 10.3 Å. The critical interaction distance for cross relaxation can be found from the data given in Ref. 4 adjusted to correspond to our Eq. (1). The results give $R_{\mathrm{cr}}=6$ Å. Using these values in Eq. (6) gives the predicted values for the fluorescence quantum efficiency shown as the solid line in Fig. 3. The broken line in Fig. 3 was obtained from Eq. (6) with $W=0$ and represents the theoretical prediction for η if the static cross relaxation is considered to be the only process responsible for the concentration quenching of the $^3H_4$ level. Both theoretical curves were obtained with no adjustable parameters.

The differences in the experimental points from different research groups are associated with how accurately the Tm concentrations in the samples are known. It is not clear from Refs. 4 and 10 how these concentrations were measured. If the results from all of the research groups are treated equally, the solid line in Fig. 3 gives the best fit to the data. If the quoted concentrations are those in the initial melt used for crystal growth instead of values measured in the actual sample, they provide a high estimate for the concentration of Tm in the crystal. If this is the case, the solid line in Fig. 3 will be a much better fit than the broken line. Thus it appears that some energy migration is taking place in the $^3H_4$ level of Tm^{3+} and this enhances the cross-relaxation quenching of the luminescence from this level especially at high Tm ion concentrations.

B. Tm-Tm migration in the $^3F_4$ level

After relaxation to the $^3F_4$ level, long-range energy migration occurs. This process was investigated using LIG spectroscopy and preliminary results were published earlier.[16] The laser write beams resonantly excite the $^1G_4$ level of the Tm ions after which there is radiative and nonradiative relaxation to the $^3F_4$ level. The properties of the LIG transient decay kinetics provide information about the excitation migration among Tm ions in the metastable state. To model the LIG decay dynamics, the generalized master equation (GME) theory developed by Kenkre[17] was used. For transient LIG signals exhibiting exponential decays, the time dependence of the signal is given by[17]

$$S(t)=S(0)\exp\{-2t[((\alpha+1/\tau)^2+16V^2\sin^2(\pi d/\Lambda))^{1/2}-\alpha]\}\ , \tag{8}$$

where V is the nearest-neighbor interaction rate causing the excitation migration, α is the excitation scattering rate, d is the nearest-neighbor distance, Λ is the grating spacing $\Lambda=\lambda/[2\sin(\theta/2)]$, λ and θ are the wavelength and the crossing angle of the write beams, respectively, and τ is the excitation lifetime. Equation (8) was fit to the measured transient LIG signal decays, treating V and α as adjustable parameters. The distance d was taken to be the average nearest-neighbor distance between Tm^{3+} ions assuming a random distribution. This is given by[18]

$$d=0.55n_{\mathrm{Tm}}^{-1/3}\ . \tag{9}$$

The LIG decay kinetics were investigated for several grating spacings and for a variety of temperatures and Tm^{3+} ion concentrations. Typical values of α and V obtained from fitting Eq. (8) to these data are listed in Table III, where the ± error bars express the sensitivity of the fit to the listed values of the adjustable parameters. It should be pointed out that the fits were not unique, but other values of α and V that gave equivalent fits to the data had magnitudes that were not physically reasonable for these parameters.

A theoretical estimate for the ion-ion interaction rate can be obtained using the Forster decay function[14]

$$\varphi(t)=\exp(-\gamma t^{1/2})\ , \tag{10}$$

where γ is given by Eq. (4). For the case of interest here R_{cr}, in Eq. (4) is replaced by the critical interaction distance for migration in the $^3F_4$ level. If we consider the excitation migration as a nearest-neighbor hopping process, an average ion to ion hopping time can be defined as

$$\varphi(\tau_{\mathrm{hop}})=e^{-1} \tag{11}$$

and an average ion-ion interaction rate can be calculated using Eqs. (10) and (11),

$$(\tau_{\mathrm{hop}})^{-1}=\gamma^2\ . \tag{12}$$

TABLE III. Excitation migration parameters at room temperature.

Sample No.	α 10^3 s^{-1}	V 10^3 s^{-1}	D cm^2/s	L_m 10^{-8} cm	L_D 10^{-5} cm	N_S
1	5.0±2.0	170±30	3.0×10^{-8}	240.4	2.19	48
2	1.5±0.6	62±12	1.8×10^{-8}	344.9	1.53	58.5
3	0.7±0.3	27±6	0.9×10^{-8}	365.5	1.34	54.5

Using Eq. (1) and the spectra in Fig. 4, the critical interaction distance for energy migration in the $^3F_4$ level was calculated to be 16 Å. This value is smaller than the value of 21 Å reported by Armagan *et al.*[4] for the same migration process. The discrepancy may be due to the fact that the authors of Ref. 4 used an equation to calculate the critical interaction distance that differed from the standard Forster equation used here by a factor of n^5.

Figure 8 shows a plot of the nearest-neighbor interaction rate V versus Tm concentration. The solid circles represent the values of V determined from fitting Eq. (8) to the experimental data. The line represents the theoretical prediction for the average ion-ion interaction rate calculated using Eq. (12). The value used for A_r was 90.9 s^{-1}. This was obtained from the fluorescence lifetime of the Tm $^3F_4$ level measured in a lightly doped sample (sample 4) and should be a good approximation of the intrinsic radiative decay rate of this level. This value is slightly lower than the value of 109.9 s^{-1} obtained from Judd-Ofelt calculations.[12] As can be seen in Fig. 8, there is a good agreement between the values of V determined from experimental data and those predicted theoretically.

The ion-ion interaction rate and the excitation scattering rate can be used to calculate the parameters describing the excitation migration properties. These parameters are the diffusion coefficient

$$D=2V^2d^2/\alpha \ , \tag{13}$$

the mean-free path

$$L_m=(2)^{1/2}Vd/\alpha \ , \tag{14}$$

the diffusion length

$$L_D=(2D\tau)^{1/2} \ , \tag{15}$$

and the number of sites visited between scattering events

$$N_S=L_m/d \ . \tag{16}$$

The values obtained for these parameters for each of the samples investigated are listed in Table III. These values show that, for each sample, $\alpha < V$, and $d < L_m \ll \Lambda$. Thus the excitation migration in these samples is a long mean-free-path type of random walk instead of a migration in which each step of the random walk involves a scattering event.

The values of the excitation migration parameters for sample 2 which is co-doped with Ho ions can be used to estimate the overall energy transfer rate from the Tm to the Ho ions. Assuming a simple model of excitation hopping to the nearest neighbor (which may be either Tm^{3+} or Ho^{3+}), the probability per unit time of making a hop is given by

$$P_{\text{hop}}=N_S\alpha \ . \tag{17}$$

Assuming the ions are uniformly distributed, the probability that a hop is to a Ho ion is $\frac{1}{12}$ (from the ratio of the Tm and Ho ion concentrations in sample 2). The energy transfer rate from the donors (Tm ions) to the acceptors (Ho ions) can then be calculated using Eqs. (17), (16), and (14) to be

$$K_{\text{Tm-Ho}}=(2)^{1/2}V/12 \ . \tag{18}$$

This equation predicts an energy transfer rate of $K_{\text{Tm-Ho}}=7.3\times10^3\ s^{-1}$.

LIG decay kinetics were measured in sample 1 at several different temperatures. Figure 9 shows the results obtained for variation of the ion-ion interaction rate, V, with temperature. The open circles represent the values of V obtained from fitting Eq. (8) to the transient LIG signal decay curves. Using Eq. (1) and the spectra in Fig. 6, the critical interaction distance at a temperature of 12 K for the Tm $^3F_4$ migration process was calculated to be 11.5 Å. This value was used in Eq. (12) to calculate

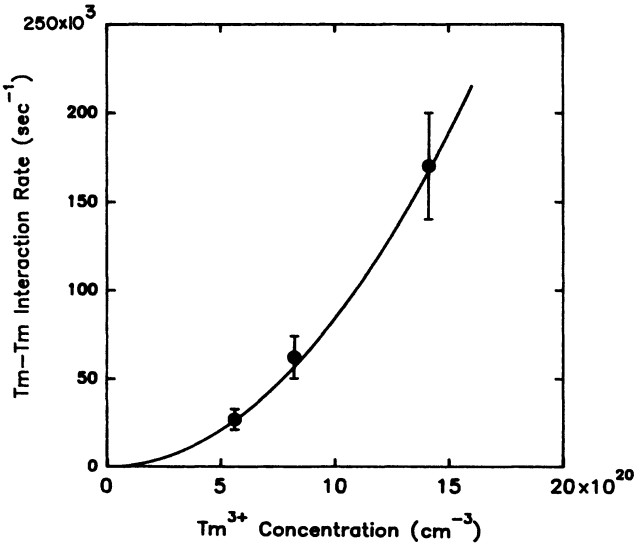

FIG. 8. Variation of the ion-ion interaction rate with Tm concentration in the $^3F_4$ migration process at room temperature. Solid circles—experimental points, line—theoretical prediction.

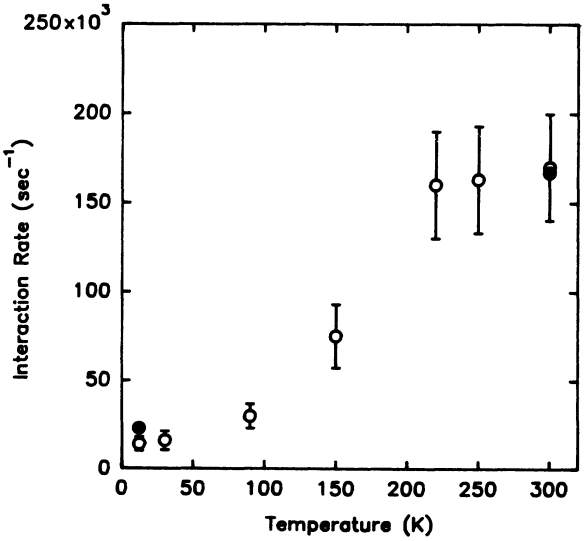

FIG. 9. Variation of the ion-ion interaction rate with temperature in the $^3F_4$ migration process for sample No. 1. Open circles—experimental points, solid circles—theoretical values.

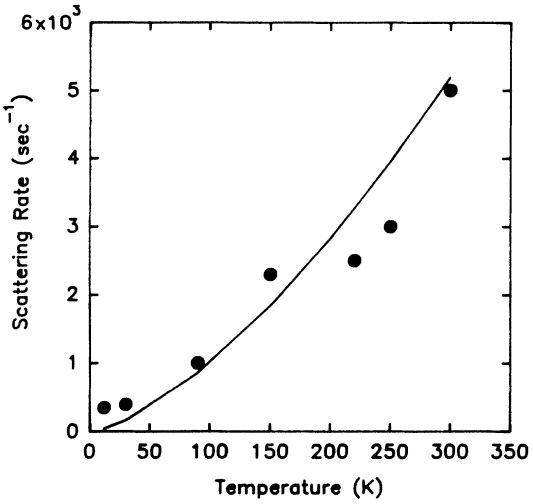

FIG. 10. Variation of the excitation scattering rate with temperature for the $^3F_4$ migration process for sample No. 1. Solid circles—experimental points, solid line—theoretical prediction.

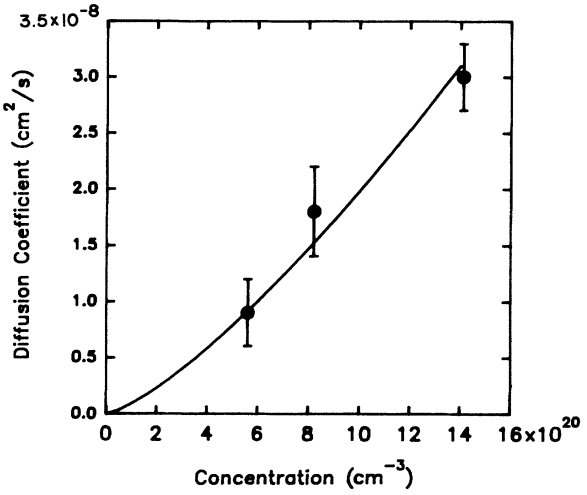

FIG. 11. Variation of the diffusion coefficient for energy migration in the Tm $^3F_4$ level with Tm concentration at room temperature. Circles—experimental values, line—theoretical prediction.

theoretical predictions for the ion-ion interaction rate at 12 K. The solid circles represent the ion-ion interaction rates predicted by Eq. (12). As can be seen in Fig. 9, the ion-ion interaction rate decreases as temperature is lowered. The good agreement between the theoretical prediction and the experimental result at 12 K, indicates that this decrease is due to the decrease in the value of the critical interaction distance due to a decrease in the spectral overlap integral as temperature is lowered.

Figure 10 shows a plot of the excitation scattering rate, α, versus temperature. The solid circles are values of α obtained from fitting Eq. (8) to the transient LIG signal decay curves. The possible excitation scattering mechanisms include scattering by defects, optical phonons, and acoustic phonons. Each of these processes has a different temperature dependence. Scattering by acoustic phonons is generally the dominant mechanism at low temperatures. This type of scattering results in a predicted temperature dependence[19] of $\alpha \propto T^{3/2}$. The solid line in Fig. 10 represents a best fit to the experimental points assuming a $T^{3/2}$ dependence. As can be seen in Fig. 10, this theory provides a reasonable prediction for the observed variation of α with temperature.

The concentration dependence of the diffusion coefficients for energy migration in the $^3F_4$ level of the Tm ions determined from LIG analysis is shown in Fig. 11. The circles are values calculated from experimental results and the line represents the best fit to the experimental points assuming an $n_{\mathrm{Tm}}^{4/3}$ dependence. As can be seen in Fig. 11, this prediction is in good agreement with the observed results. This type of concentration dependence is predicted by all of the theories developed to describe a random walk type of excitation migration.[15,17,20,21]

C. Tm-Ho energy transfer

The transfer of energy from the $^3F_4$ level of the Tm ions to the $^5I_7$ level of the Ho ions is the final step in the overall energy transfer in the Tm,Ho:YAG system. In a recent publication[22] we reported measurements of the rise time of the fluorescence emission from the $^5I_7$ level of the Ho ions in Tm,Ho:YAG (sample 2) after pumping the Tm^{3+} ions. The signal was found to rise from zero to a maximum value in 330±30 μs. For a nonradiative cross-relaxation energy transfer process from the Tm ions in the $^3F_4$ level to the $^5I_7$ level of the Ho ions the time in which the fluorescence emission of Ho rises to a maximum value is given by[23]

$$t_{\max}=\frac{1}{\tau_{\mathrm{Ho}}^{-1}-\tau_{\mathrm{Tm}}^{-1}-\omega_{\mathrm{cr}}}\left[\ln\left[\frac{\tau_{\mathrm{Ho}}^{-1}}{\tau_{\mathrm{Tm}}^{-1}+\omega_{\mathrm{cr}}}\right]+\frac{\tau_{\mathrm{Ho}}^{-1}(\tau_{\mathrm{Tm}}^{-1}+\omega_{\mathrm{cr}}-\tau_{\mathrm{Ho}}^{-1})}{(\tau_{\mathrm{Tm}}^{-1}+\omega_{\mathrm{cr}})\omega_{\mathrm{cr}}}[n_2(0)/N_2(0)]\right], \tag{19}$$

where τ_{Tm}^{-1} is the intrinsic decay rate of the Tm $^3F_4$ level, τ_{Ho}^{-1} is the intrinsic decay rate of the Ho $^5I_7$ level, and ω_{cr} is the cross-relaxation rate between the two systems of ions. $N_2(0)$ is the number of Tm ions initially in the $^3F_4$ level and $n_2(0)$ is the number of Ho ions initially in the $^5I_7$ excited state. Since, in our case, $n_2(0)=0$, Eq. (19) takes the simple form

$$t_{\max}=\frac{1}{\tau_{\mathrm{Ho}}^{-1}-\tau_{\mathrm{Tm}}^{-1}-\omega_{\mathrm{cr}}}\ln\left[\frac{\tau_{\mathrm{Ho}}^{-1}}{\tau_{\mathrm{Tm}}^{-1}+\omega_{\mathrm{cr}}}\right]. \tag{20}$$

Using the experimentally measured value for $t_{\max}$, of 330

μs, a value of 6.5 ms for the intrinsic lifetime of the $^5I_7$ energy level of Ho^{3+} in YAG,[24] and a value of 11 ms for the fluorescence lifetime of the Tm $^3F_4$ level in YAG, Eq. (20) predicts a value for the energy transfer rate of $\omega_{cr}=1.3\times10^4$ s^{-1}. The value used for τ_{Tm} was measured in sample 4.

The value obtained here for the overall Tm-Ho transfer rate is within a factor of 2 of the value calculated in Sec. IV B using the excitation migration parameters determined from LIG analysis. Considering the simplifying approximations used in both approaches, these results are in reasonably good agreement. One obvious simplification in the excitation hopping model is the assumption that the ions are uniformly distributed. Effects of nonuniform ion distributions and inhomogeneous broadening can affect the value derived for the overall energy transfer rate.

Energy transfer theories that account specifically for both energy migration among donors and transfer to acceptors[15,20,21] were employed to calculate theoretical predictions for the overall Tm-Ho transfer rate using the data in Table II. The transfer rates calculated using these theories are 3–4 times lower than the value obtained from experimental data using Eq. (20). The diffusion coefficients for energy migration among the donors (Tm ions) predicted by these models[15,20] are of the order of 10^{-10}–10^{-11} cm^2/s which is more than 2 orders of magnitude smaller than the measured values. The large discrepancy between the predicted values of D and those obtained from the experimental results in Sec. IV B may be partly due to the fact that these theoretical models consider the excitation migration among the donor ions as a process in which a scattering event occurs on every hop of the excitation to another site. This corresponds to excitation migration parameters, $\alpha\simeq V$. However, the analysis of the LIG data obtained here has shown that $\alpha\ll V$ for the samples investigated here.

V. CONCLUSIONS

The results described here provide an extensive characterization of the energy transfer and migration processes in Tm,Ho:YAG crystals. This is the first investigation that has characterized each of the individual ion-ion interaction processes separately and shown how their combined effects lead to the efficient Tm sensitization of Ho luminescence that has been observed experimentally.

The results indicate that there is some energy migration taking place in the Tm $^3H_4$ level and this enhances the cross-relaxation process that is responsible for the fluorescence quenching of this level. This migration is especially important at high levels of Tm ion concentration and has not been previously characterized. Since cross relaxation from the $^3H_4$ level is important in enhancing the quantum efficiency of the system by providing two excited ions for one absorbed pump photon, understanding this process is critical to determining the optimum concentration of Tm ions for maximizing the sensitization process. It should be pointed out that the excitation migration in the $^3H_4$ level of the Tm ions makes no discernible contribution to the measured decay characteristics of the LIG's in any of the samples investigated. This is demonstrated by the fact that the excitation lifetime in the $^3H_4$ level is of the order of several microseconds, while the excitation lifetime in the $^3F_4$ level and the decay times of the LIG's are on a millisecond time scale. Thus the short-lived excitation in the $^3H_4$ level does not migrate over long enough distances to alter the laser-induced population grating pattern.

The dominant process of spatial energy migration was found to occur in the Tm $^3F_4$ level. The results of LIG spectroscopy show that this process occurs through a long mean-free-path random walk in which the migrating excitation is scattered by acoustic phonons. The ion-ion interaction rate causing each step in the random walk is accurately described by an electric dipole-dipole mechanism. This decreases at low temperatures as the spectral overlap that characterizes the resonant interaction between neighboring ions decreases. The temperature and Tm ion concentration dependences of the results are accurately described by this model.

The overall Tm-Ho energy transfer rate was calculated using the excitation migration parameters described above. A simple model assuming the Ho ions act as traps for the migrating Tm ion excitation gives a reasonable agreement with the transfer rate measured from fluorescence spectral dynamics. The trapping step is consistent with the prediction of an electric dipole-dipole interaction mechanism that deexcites the Tm ion in the $^3F_4$ level and excites the Ho ion to the $^5I_7$ level. The rate of this interaction step is greater than the rate of the Tm-Tm migration step, and thus the overall transfer is a diffusion-limited process.

It is known that back transfer from the $^5I_7$ level of the Ho ions to the $^3F_4$ level of Tm ions is efficient enough to lead to the condition of thermal equilibrium of the populations of these two excited states.[1,3,8] The equilibration time has been measured to be about 200 μs in a sample of similar Tm and Ho concentrations as sample no. 2 in this work.[3] Since the decay times of the LIG signals measured in this work were of the order of a few milliseconds, the presence of back transfer will simply decrease the trapping efficiency of the migrating Tm excitation energy, and not influence the dynamics of the grating decay.

The efficient transfer of energy to the Ho ions can also produce a polarizability change while the ions are in the $^5I_7$ level. However, the intensity of LIG signal is proportional to the square of the excited state population.[9] Since the concentration of the Ho ions in sample 2 is 12 times smaller than that of the Tm ions, the contribution of the Ho ion polarizability change to the observed LIG signal will be over 2 orders of magnitude smaller than the contribution to the signal made by the Tm ions. Thus this contribution will be negligible. In addition, the low concentration of Ho ions inhibits any spatial migration of energy in their $^5I_7$ metastable states. The ion-ion interaction rate between the Ho ions is estimated to be at least an order of magnitude smaller than that between Tm ions. Thus energy migration among the Ho ions plays no role in the LIG decay dynamics.

The results described here provide a detailed under-

standing of all of the important processes involved in the optical pumping dynamics of laser-pumped Tm,Ho:YAG lasers. A rate equation model based on the transitions shown in Fig. 1 has been developed to predict the operational characteristics of these lasers.[22] Using all of the parameters obtained in this investigation plus other measured spectral parameters, the laser characteristics are accurately predicted with no adjustable parameters. This relationship between spectroscopic parameters and laser characteristics provides the capability for using computer modeling to predict optimum dopant concentrations, optimum laser pump wavelength, and optimum host parameters for obtaining the best laser operational parameters.[22]

ACKNOWLEDGMENTS

This research was supported by the U.S. Army Research Office and the National Science Foundation under Grant No. DMR-9103648. The authors gratefully acknowledge helpful discussions with M. G. Jani, S. A. Payne, and T. Basiev. Two of the authors (V.A.F. and R.R.P.) acknowledge the support provided by the U.S. Department of Education.

[1]See, for example, T. Y. Fan, G. Huber, R. L. Byer, and P. Mitzscherlich, IEEE J. Quantum Electron. **24**, 924 (1988).

[2]J. K. Tyminski, D. M. Franich, and M. Kokta, J. Appl. Phys. **65**, 3181 (1989).

[3]G. Armagan, A. M. Buoncristiani, and B. Di Bartolo, J. Lumin. **48-49**, 171 (1991).

[4]G. Armagan, A. M. Buoncristiani, and B. Di Bartolo, Opt. Mater. **1**, 11 (1992).

[5]G. J. Quarles, A. Rosenbaum, C. L. Marquardt, and L. Esterowitz, Appl. Phys. Lett. **55**, 1062 (1989).

[6]M. J. Jani, R. R. Reeves, R. C. Powell, G. J. Quarles, and L. Esterowitz, J. Opt. Soc. Am. B **8**, 741 (1991).

[7]A. Brenier, J. Rubin, R. Moncorge, and C. Pedrini, J. Phys. (Paris) **50**, 1463 (1989).

[8]S. A. Payne, L. K. Smith, W. L. Kway, and W. F. Krupke, J. Phys. Condens. Matter (to be published).

[9]R. C. Powell, S. A. Payne, L. L. Chase, and G. D. Wilke, Phys. Rev. B **41**, 8593 (1990).

[10]T. Becker, R. Clausen, G. Huber, E. W. Duczyski, and P. Mitzerlich, in *Tunable Solid State Lasers,* edited by M. L. Shaud and H. P. Jenssen (Optical Society of America, Washington, D.C., 1989), Vol. 5, p. 150.

[11]D. L. Dexter, J. Chem. Phys. **21**, 836 (1953).

[12]J. A. Caird, L. G. DeShazer, and J. Nella, IEEE J. Quantum Electron. **11**, 874 (1975).

[13]J. A. Caird, A. J. Ramponi, and P. R. Staver, J. Opt. Soc. Am. B **8**, 1391 (1991).

[14]T. Forster, Ann. Phys. (N.Y.) **2**, 55 (1948); Z. Naturforsch. **49**, 321 (1949).

[15]A. I. Burshtein, Zh. Eksp. Teor. Fiz. **62**, 1695 (1972) [Sov. Phys. JETP **35**, 882 (1972)]; **84**, 2001 (1983) [**57**, 1165 (1983)]; M. V. Artamonova, C. M. Briskina, A. I. Burshtein, L. D. Zusman, and A. G. Skleznev, *ibid.* **62**, 863 (1972) [**35**, 457 (1972)].

[16]V. A. French and R. C. Powell, Opt. Lett. **16**, 666 (1991).

[17]V. M. Kenkre and D. Schmid, Phys. Rev. B **31**, 2430 (1985); V. M. Kenkre, Phys. Rev. B **18**, 4064 (1978).

[18]S. Chandrasekhar, Rev. Mod. Phys. **15**, 1 (1943).

[19]V. M. Agranovich and M. D. Galanin, *Electronic Excitation Energy Transfer in Condensed Matter* (North-Holland, Amsterdam, 1982).

[20]D. L. Huber, Phys. Rev. B **20**, 2307 (1979); **20**, 5333 (1979); **22**, 1714 (1980).

[21]A. Blumen and R. Silbey, J. Chem. Phys. **70**, 3707 (1979).

[22]R. R. Petrin, M. G. Jani, R. C. Powell, and M. Kokta, Opt. Mater. **1**, 111 (1992).

[23]R. C. Powell, B. DiBartolo, B. Birang, and C. S. Naiman, Phys. Rev. **155**, 296 (1967).

[24]G. M. Zverev, G. Y. Kolodnyi, and A. M. Onishchenko, Zh. Eksp. Teor. Fiz. **57**, 794 (1969) [Sov. Phys. JETP **30**, 435 (1970)].